NANO LETTERS

2008
Vol. 8, No. 1
6−12

Systematic Study on Quantum Confinement and Waveguide Effects for Elastic and Inelastic Currents in Atomic Gold Wire: Importance of the Phase Factor for Modeling Electrodes

Hisao Nakamura* and Koichi Yamashita

Department of Chemical System Engineering, Graduate School of Engineering, The University of Tokyo, Tokyo 113-8656, Japan

Received May 31, 2007; Revised Manuscript Received November 5, 2007

ABSTRACT

Quantum confinement of the electrodes is an important issue for electron transport through molecular or atomic wire junctions. To assess the importance of waveguide effects by quantum confinement of the electrodes, we have calculated elastic and inelastic conductance and inelastic electron tunneling spectra of atomic gold wire with gold electrodes for several models. The results show the quite important role of the phase factors between the modeled electrodes and the contact region.

There has been progress in conduction by atomic wires or molecular junctions toward applications to new devices[1−5] and single-molecule spectroscopic techniques,[6−11] such as inelastic tunneling spectroscopy (IETS). Generally, it is difficult to manipulate or specify atomic structure for the junction (contact region) experimentally, and several groups have performed ab initio calculations of transport for realistic electrode−molecule−electrode systems.[12−17] In many cases, analyses have been mainly focused on the properties of the contact region.[18] Theoretical treatment of the electrodes often depends on an adopted model of the contact region and ab initio method, such as cluster approximation or periodic slab,[19,20] and electrodes are modeled by a one-dimensional (1-D) rod or a semi-infinite surface with two-dimensional (2-D) periodicity. However, strictly speaking, the two models relate to physically different systems and are relevant to different experiments. Recently, Ke et al. showed that the behavior of transport through the whole system depends not only on contact but also on the electrode itself as a result of quantum confinement.[21,22] In this letter, we report the above quantum confinement and waveguide effects on change of conductance and IETS caused by electron−phonon scattering and show the importance of the correct modeling of electrodes for theoretical treatments. Throughout this report, we adopt a nonequilibrium Green's function (NEGF) approach combined with density functional theory (DFT),[23−25] including electron−phonon interaction within the lowest-order expansion (LOE) framework.[26−29]

The parts of the semi-infinite electrode are incorporated into the central (C) region by using self-energy matrices. By enforcing 1-D nonperiodicity or 2-D periodicity parallel to the surface, the following three models can be considered for the C region illustrated in Figure 1a:

Model (I): 2-D periodic contact + 2-D periodic leads

Model (II): 1-D contact + 2-D periodic leads

Model (III): 1-D contact + 1-D leads

When the unit cell is sufficiently large, the 2-D periodic structure can be regarded as effectively infinite surface electrodes, and the interaction between chain parts can be negligible. As a result, one can consider that models (I)−(III) correspond to the physical situations, which are illustrated in the insets in Figures 2a, 3a, and 4a, respectively. Physically, model (I), where the contact connects to clean surfaces, will be relevant to the extremely ideal cases for surface STM/AFM experiments or a mechanically controllable break junction (MCBJ) technique, while model (II) will be a much more realistic experimental case. Model (III) relates to the 1-D rod system.

Theoretical Background. When a vibrational mode Q_α is obtained in the C region (or in a subspace of C by means of the frozen phonon approximation), the phonon scatterings are included in the self-energy terms. In terms of the electron−phonon coupling M^α, the self-energy terms of electron−phonon interactions are represented by[29−31]

* To whom correspondence should be addressed. E-mail: nakamura@tcl.t.u-tokyo.ac.jp.

10.1021/nl071281c CCC: $40.75
Published on Web 12/15/2007

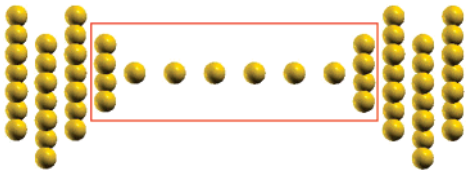

Figure 1. The atomic structure of the gold wire in the Au(100) systems, where the unit cell is a 3 × 3 structure, is shown. The unit is treated with/without the periodic boundary condition in each model, as well as the electrodes. The part enclosed by the solid line is the "vibrational box".

$$\Sigma^{<}_{\mathrm{eph}}(E) = \frac{i}{2\pi}\int \mathrm{d}\omega\{D^{<}_{\alpha}(\omega)M^{\alpha}G^{<}(\epsilon-\omega)M^{\alpha}\} \quad (1a)$$

$$\Sigma_{\mathrm{eph}}(E) = \frac{i}{2\pi}\int \mathrm{d}\omega\{D^{<}_{\alpha}(\omega)M^{\alpha}G^{\dagger}(\epsilon-\omega)M^{\alpha} + D^{\dagger}_{\alpha}M^{\alpha}G^{>}(\epsilon-\omega)M^{\alpha} - D_{\alpha}(0)M^{\alpha}\mathrm{Tr}[G^{<}(\omega)M^{\alpha}]\} \quad (1b)$$

where $G(E)$ and $D_\alpha(\omega)$ are Green's functions for the electron and phonon, respectively. The symbols "<" and ">" represent lesser and greater Green's functions, respectively. Throughout this study, we use the molecular orbital (MO) basis to expand (electronic) Green's functions instead of the atomic orbital (AO) basis set, where the MOs are defined on the C region. The current $I(V)$, differential conductance, $G(V) = \mathrm{d}I/\mathrm{d}V$, and IETS signal, $\mathrm{d}^2I/\mathrm{d}V^2$, can be calculated as a function of the voltage V using Green's functions and self-energies. The applied voltage and the Fermi levels of the left and right leads, μ_L and μ_R, satisfy the condition $eV = \mu_L - \mu_R$, where e is the absolute value of the electron charge.

Recently, we developed a NEGF-DFT scheme called the "efficient MO approach"[23] and used it for the present calculation. Details of the scheme and procedure will be given elsewhere.[32] By using eq 1a,b and applying the LOE approximation, the total current can be represented as the sum of the elastic I^{el} and inelastic I^{inel} currents, and the elastic part is further separated into the ballistic term I^{el}_0 and the remaining term δI^{el}, which relates to the elastic electron−phonon scatterings.[15,26−29] In the present study, we implemented the LOE form derived by Viljas et al., and details are given in ref 29.

The terms I^{el}_0, δI^{el}, and I^{inel} are expressed in terms of the $G(E)$ obtained by the result of ballistic NEGF-DFT as follows

$$I^{\mathrm{el}}_0 = G_0\int \mathrm{d}E T_0(E)(f_L(E) - f_R(E)) \quad (2a)$$

$$\delta I^{\mathrm{el}} = -\int \mathrm{d}E\left[\sum_{\sigma=\pm}\sigma\int_0^{\infty}\mathrm{d}\omega\frac{1}{\pi}\mathrm{Im}D_\alpha(\omega)\{T^{\mathrm{ec}}_{\sigma\alpha}N_\alpha(\sigma\omega) + T^{\mathrm{ecL}}_{\sigma\alpha}f_L(E_{\sigma\alpha}) + T^{\mathrm{ecR}}_{\sigma\alpha}f_R(E_{\sigma\alpha})\}\{f_L(E) - f_R(E)\}\right] - \int \mathrm{d}E\left[\int_{-\infty}^{\infty}\mathrm{d}\omega\frac{1}{\pi}\mathrm{Re}D_\alpha(\omega)\{T^{\mathrm{asyL}}_{\alpha}f_L(E-\omega) + T^{\mathrm{asyR}}_{\alpha}f_R(E-\omega)\}\{f_L(E) - f_R(E)\}\right] \quad (2b)$$

$$I^{\mathrm{inel}} = -\int \mathrm{d}E\left[\sum_{\sigma=\pm}\sigma\int_0^{\infty}\mathrm{d}\omega\frac{1}{\pi}\mathrm{Im}D_\alpha(\omega)T^{\mathrm{in}}_{\sigma\alpha}\{N_\alpha(\sigma\omega)f_L(E)[1 - f_R(E_{\sigma\alpha})] + N_\alpha(-\sigma\omega)f_R(E_{\sigma\alpha})[1 - f_L(E)]\}\right] \quad (2c)$$

where $\Gamma_{L/R}$ relates to the left and right lead self-energy matrices $\Sigma_{L/R}$

$$\Gamma_{L/R} = -2\mathrm{Im}\Sigma_{L/R} \quad (3)$$

and $f_{L/R}$ is the Fermi function. The factor G_0 is the unit of quantized conductance, $e/\pi\hbar$, where $\hbar$ is the Planck constant. The (ballistic) transmission coefficient is expressed by

$$T_0(E) = \mathrm{Tr}[G(E)\Gamma_R(E)G^{\dagger}(E)\Gamma_L(E)] \quad (4)$$

The correction terms for the elastic current are represented by factors T^{ec}, $T^{\mathrm{ecL/R}}$, and $T^{\mathrm{asyL/R}}$ as follows

$$T^{\mathrm{ec}}_{\sigma\alpha}(E,\omega) = 2G_0\mathrm{ReTr}[M^{\alpha}G(E_{\sigma\alpha})M^{\alpha}G(E)\Gamma_R(E)G^{\dagger}(E)\Gamma_L(E)G(E)] \quad (5a)$$

$$T^{\mathrm{ecL/R}}_{\sigma\alpha}(E,\omega) = G_0\mathrm{ImTr}[M^{\alpha}G(E_{\sigma\alpha})\Gamma_{L/R}(E_{\sigma\epsilon})G^{\dagger}(E_{\sigma\alpha})M^{\alpha}G(E)\Gamma_R(E)G^{\dagger}(E)\Gamma_L(E)G(E)] \quad (5b)$$

$$T^{\mathrm{asyL/R}}_{\alpha}(E,\omega) = G_0\mathrm{ReTr}[M^{\alpha}G(E-\omega)\Gamma_{L/R}(E-\omega)G^{\dagger}(E-\omega)M^{\alpha}G(E)] \quad (5c)$$

Here, we introduce the notation $E_{\sigma\alpha}$, which represents $E \pm \Omega_\alpha$ for $\sigma = \pm 1$, respectively. The factor in the inelastic term is also expressed by using $T^{\mathrm{in}}_{\sigma\alpha}(E,\omega)$ as follows

$$T^{\mathrm{in}}_{\sigma\alpha}(E,\omega) = G_0\mathrm{Tr}[M^{\alpha}G(E_{\sigma\alpha})\Gamma_R(E_{\sigma\alpha})G^{\dagger}(E_{\sigma\alpha})M^{\alpha}G^{\dagger}(E)\Gamma_L(E)G(E)] \quad (6)$$

Equations 5 and 6 contain the voltage-dependent phonon occupation function N_α.

In the present study, we omit coupling between the phonon mode α and other modes though electron and phonon temperature are fixed at 15 K and the broadening parameter is set to 20 meV. Thus, the phonon occupation is also calculated to the second order of M^{α} by using the lesser and retarded self-energies of the phonon.

Computational Model. In the present study, the C region consists of a chain part of six Au atoms, a 2 × 2 top layer, and three additional (i.e., the second−fourth) layers, which connect to the semi-infinite electrodes of the (100) surface (see Figure 1a). For these additional layers and electrodes, we took the 3 × 3 surface first and then performed similar calculations using the 4 × 4 system.

The geometry of the (100) layers is fixed with a lattice constant of 4.08 Å, and the distance between each second layer is kept at 21.90 Å. Only the chain and top layers of each side (a total of 14 atoms) are relaxed, and the vibrational modes are calculated in this "vibrational box". Here, we note

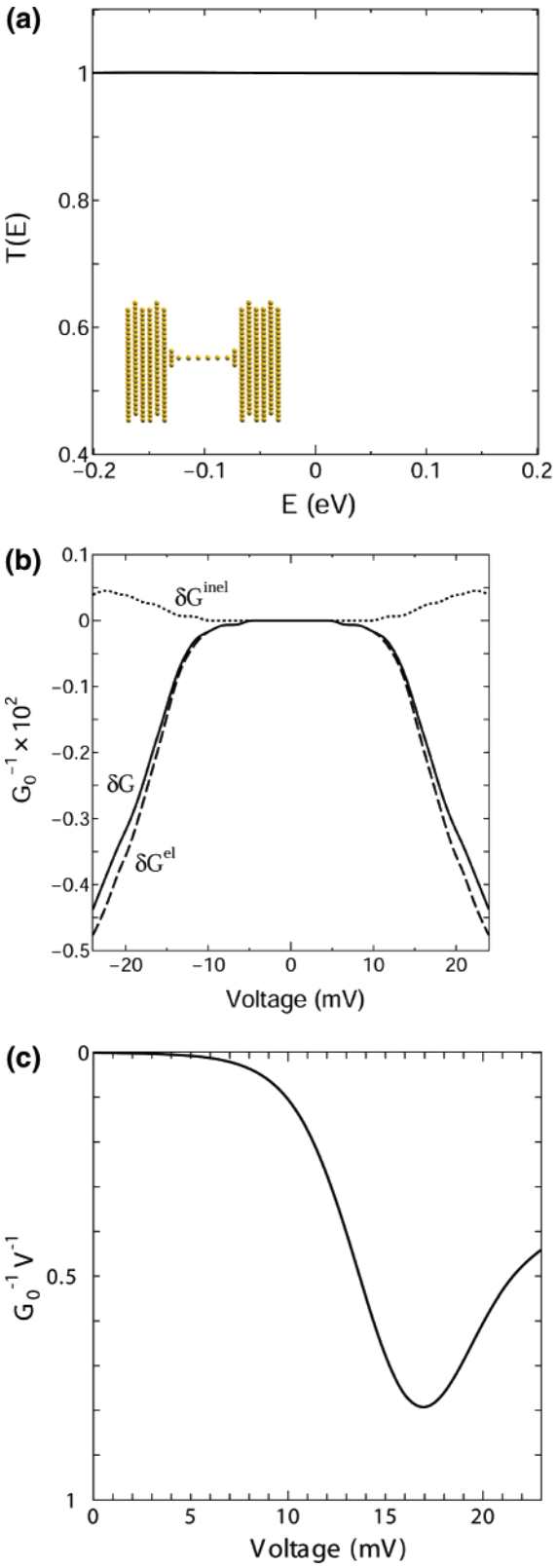

Figure 2. The ballistic transmission coefficient $T_0(E)$, the changes of conductance by electron−phonon scatterings, and the IETS signal in model (I). $T_0(E)$ in the zero bias limit is plotted as a function of electron energy in (a), where the Fermi level is set to zero. The inset represents a schematic figure of a physical system related to the adopted periodic (or nonperiodic) boundary condition. The change of conductance is given as a function of the voltage in (b). The total change δG is shown by the solid line, and elastic (δG^{el}) and inelastic (δG^{inel}) terms are given by the dashed and dotted lines, respectively. The IETS signal of the ABL mode is given in (c).

that we take a much larger region (W) than the C region to determine the first derivatives of the Hamiltonian and overlap matrices and Hessian, although only the parts relating to the C region are explicitly used. We took the W region as the C region plus the outer three layers for both the 1-D and 2-D periodic cases and obtained the converged results of the phonon frequencies and eigenmode vectors. Recent experimental and theoretical studies of atomic gold nanowires have reported that the alternating bond length (ABL) phonon mode is important to the transport process.[29,33,34] Therefore, we focus on only the highest ABL mode, which is denoted α and has the highest frequency Ω_α.

A part of the DFT calculations was performed by the SIESTA program package,[35] and PBE functions were adopted as the XC functional. The basis set employed was the AO type of the polarized single zeta (SZP) level with use of Troullier−Martins norm-conserving pseudopotential and the Kleinman−Bylander nonlocal projector.

To estimate lead self-energy terms, we adopted the tight-binding layer scheme.[24] To incorporate 1-D and 2-D periodicity for the electrodes, 1-D and 2-D periodic boundary conditions were imposed on the DFT calculation for the principle layer (PL); thus, each lead self-energy satisfies each boundary condition for the parallel direction of the surface, the same as that with the C region. In all of the calculations for both the C region and the electrodes, the Γ point approximation was used if the 2-D periodic boundary condition was required.

Model (I). Model (I) is entirely the 2-D periodic system. The atoms in the vibrational box did not almost change the positions after the geometry optimization, that is, the chain part is linear, and the structure of the top layers is almost same with the (100) section. Using this optimized geometry, we found that the frequency of the ABL mode has the value of 128.3 cm^{-1} for the 3×3 unit cell.

The calculated $T_0(E)$ was almost constant in the energy range of [−0.2, 0.2] eV and had the value 1.0 due to conduction of the 6s electron of Au in the low bias voltage as shown in Figure 2a, where we set the Fermi level to 0. In the present case, we focus on only low applied voltage (typically lower than 25 mV), and the voltage dependence of $T_0(E)$ is quite small. Therefore, we only show $T_0(E)$ of the zero bias case for all models and illustrate in the figures. Note that all NEGF-SCF calculations are performed fully self-consistently and include bias dependence explicitly. Our result of "single open channel" transmission of (linear) gold wire agrees with the previous works.[13,26,33,34]

The change of conductance caused by electron−phonon scatterings, δG, can be defined by the sum of δG^{el} and δG^{inel}, where each term is defined by $d(\delta I^{el})/dV$ and dI^{inel}/dV, respectively. The resulting δG's, and so forth, are illustrated as a function of V in Figure 2b. The elastic term dominates the conductance drop, and the decreasing is close to linear when the applied bias is larger than Ω_α. The magnitude of δG is about 0.15% of G_0 at $eV \approx \hbar\Omega_\alpha$. Our results shows good agreement with the results of previous theoretical studies, and the order of the magnitude is properly similar to the experimental values, although the experimental result

is a little larger than our result.[26,29] Since the change of conductance is very sensitive to the length of the chain, the distance between electrodes, as well as the shape of the contact, the above agreement will be sufficient to prove the validity of our calculation. The IETS signal can be expressed as $d(\delta G)/dV$ because of the small voltage dependence of $T_0(E)$. In Figure 2c, the calculated signal, which has the peak at $eV \simeq \hbar\Omega_\alpha$, is shown for the positive voltage. Comparing the conductance change, the IETS signal is a better quantity to measure the contribution of electron−phonon scatterings due to its sharp dip (for positive bias).

We also performed additional calculations of the IETS signals for a few longitudinal phonon modes, which are not ABL modes and have frequencies close to the value of the present highest ABL mode, and found that the signal caused by these modes are almost equal to 0.

Model (II). In model (II), the lead self-energies are the same as those for model (I), but the C region is 1-D nonperiodic; thus, the system has a sufficiently long finite cross section on the 2-D electrodes. We calculated Ω_α by the same procedure as that with model (I). The frequency is very close to that of the 2-D contact as well as the eigenmode vector, and the difference in the two frequencies is within only a few cm^{-1}. Furthermore, the other eigenmodes in the vibrational box also have similar values to the modes calculated in model (I). This means that quantities such as bond energies are essentially local and robust quantities, and therefore, the periodic boundary condition is not as important for these quantities if the vibrational box (i.e., focused region) is large enough to include strong couplings between the molecule (wire) and the surfaces.

$T_0(E)$ for model (II) is presented in Figure 3a. One can find the oscillation structure of $T_0(E)$ in the presented energy window; the minimum value is about 0.7. The position of the Fermi level gives a value close to the bottom of $T_0(E)$. The calculated δG is also plotted as a function of bias voltage in Figure 3b. This is a clear example of waveguide effects due to quantum confinement. In the study by Ke et al., waveguide effects for tunneling conduction were shown because the bridge part was the benzene−dithiol molecule in their study.[21] The present case shows waveguide effects on resonant conduction.

The value of δG is about 0.05% of G_0 when the voltage is close to Ω_α; thus, the electron−phonon scatterings affect the conductance drop with a somewhat smaller magnitude for model (II) than that for model (I). However, each term resulting from elastic and inelastic scatterings is quite different. Comparing with model (I), the magnitude of δG^{el} becomes small, and δG^{inel} is enhanced. Recall that the voltage bias is quite low and dT_0/dV is close to 0; thus, the difference of δG in models (I) and (II) reflects the IETS signal straightforward, that is, the observed IETS signal will give clear evidence of the difference caused by electron−phonon scatterings in the finite cross section. In Figure 3c, the calculated IETS signal is given. The intensity is about 40% of that for the case of model (I). Since the IETS signal shows a sharp dip at almost the same position of the voltage, it is more suitable than δG to compare the contribution of quantum confinement to electron−phonon scatterings.

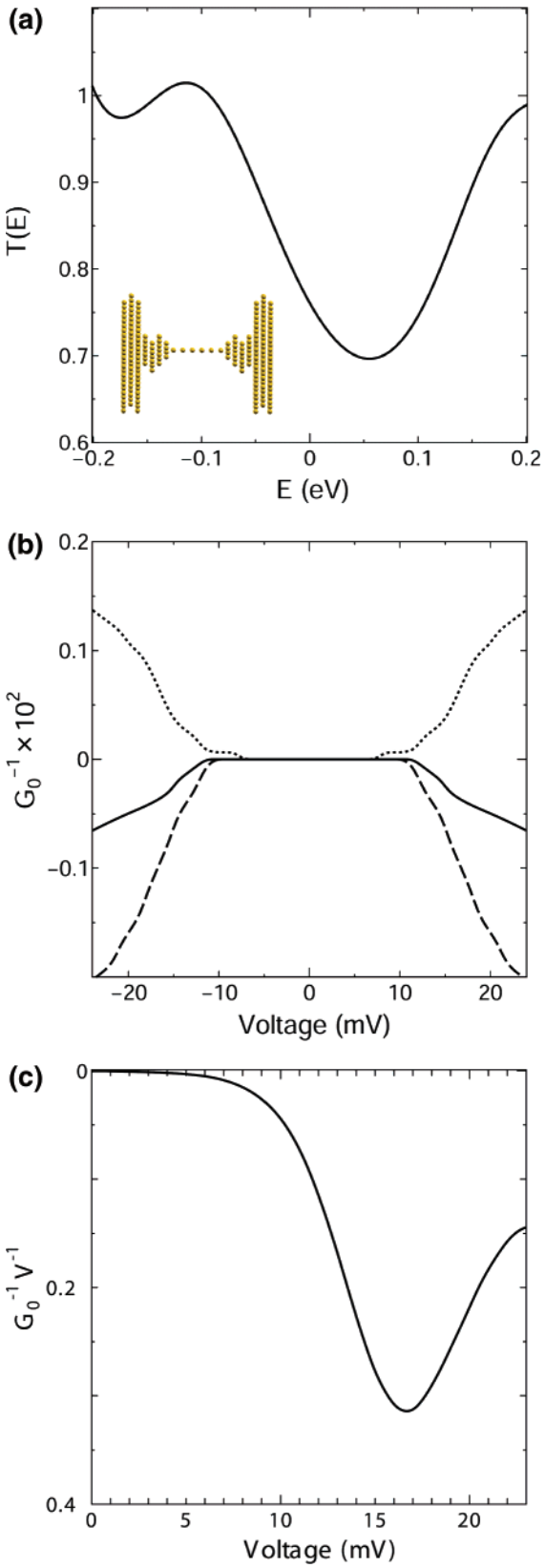

Figure 3. (a) The coefficient $T_0(E)$ and (b) the change of the conductance and (c) the IETS signal in model (II). The notations in the figures are the same as those for Figure 2.

Here, we briefly comment on the problem of van Hove singularity for the NEGF-DFT calculation, which was recently pointed out by Thygesen et al.[36] Using simple models, they showed that sharp oscillation of the transmission coefficient and density of states sometimes appears if the Γ point approximation is adopted with a small unit cell, where the periodic boundary condition is enforced. In the present system, the Γ point approximation works well for a 2-D periodic system; thus, waveguide effects caused by interference of transverse modes are more responsible for fluctuations or different magnitudes of δG, and so forth, than van Hove singularity in the present models. In the later subsection, we further analyze such interferences relating to waveguide effects.

Model (III). Model (III) is a 1-D rod, that is, an entirely 1-D nonperiodic system. The resulting $T_0(E)$ has a sharp and hard oscillation structure, as shown in Figure 4a. The peak position of $T_0(E)$ is very close to the Fermi energy. Generally, when the bias is low and the wide-band limit is acceptable, $T_0(E)$ provides the measurement that conductance is "drop" ($T_0(E) > 1/2$) or "rise" ($T_0(E) < 1/2$).[15,27,30,37] Because $T_0(E)$ is always larger than 1/2 in the present bias range, the value of δG presented in Figure 4b is negative, just as for models (I) and (II). The magnitude of the conductance drop caused by electron−phonon interactions is 2.5−3.0% of G_0 at $eV \simeq \hbar\Omega_\alpha$, which is larger than the values for the above two models.

Although δG is enhanced 15−30 times compared with models (I) and (II), much larger differences in each term for δG^{el} and δG^{inel} were found. The magnitude of δG^{el} is about 30 times as large as that for model (I) and about 150 times as that for δG^{inel}. While $T_0(E)$ is rapidly decreasing in the very narrow energy range, the change of the conductance by the ballistic term is not so rapid because the voltage dependence of $T_0(E)$ is smooth. Since the magnitude of δG^{el} is still much larger than that of δG^{inel}, the enhanced δG^{el} term provides a conductance drop of the 1-D. Recall that the electronic structure of the C region is the same with models (II) and (III); thus, the physical quantities on the C region such as electron−phonon couplings are not responsible for the difference in efficiency of vibrational heating. The local heating effects are a central issue for IETS, and the above results show the importance of using a correct model not only for the tip/contact shape but also for the structure of the cross section connected to the electrodes. In Figure 4c, the resulting IETS signal is shown. The signal shows the sharpest dip in the tree models, and the intensity is about 20 times larger than that of model (I); hence, the IETS signal will be a good physical quantity to prove clear evidence of quantum confinement relating to electron−phonon scatterings in the 3 × 3 case.

Relation between Adopted Models and Unit Cell Size. We performed the same calculation for the 4 × 4 system for models (I)−(III). In all cases, the difference of the ABL modes between the 3 × 3 and 4 × 4 systems was negligible. In model (I), a difference of $T_0(E)$ for the two cases was also negligible, and the intensity of the IETS signal for the 4 × 4 system was close to the one for the 3 × 3 system at the peak. Therefore, one can conclude that the 3 × 3 structure is of sufficient size to obtain conduction properties for the 2-D periodic case in the present system.

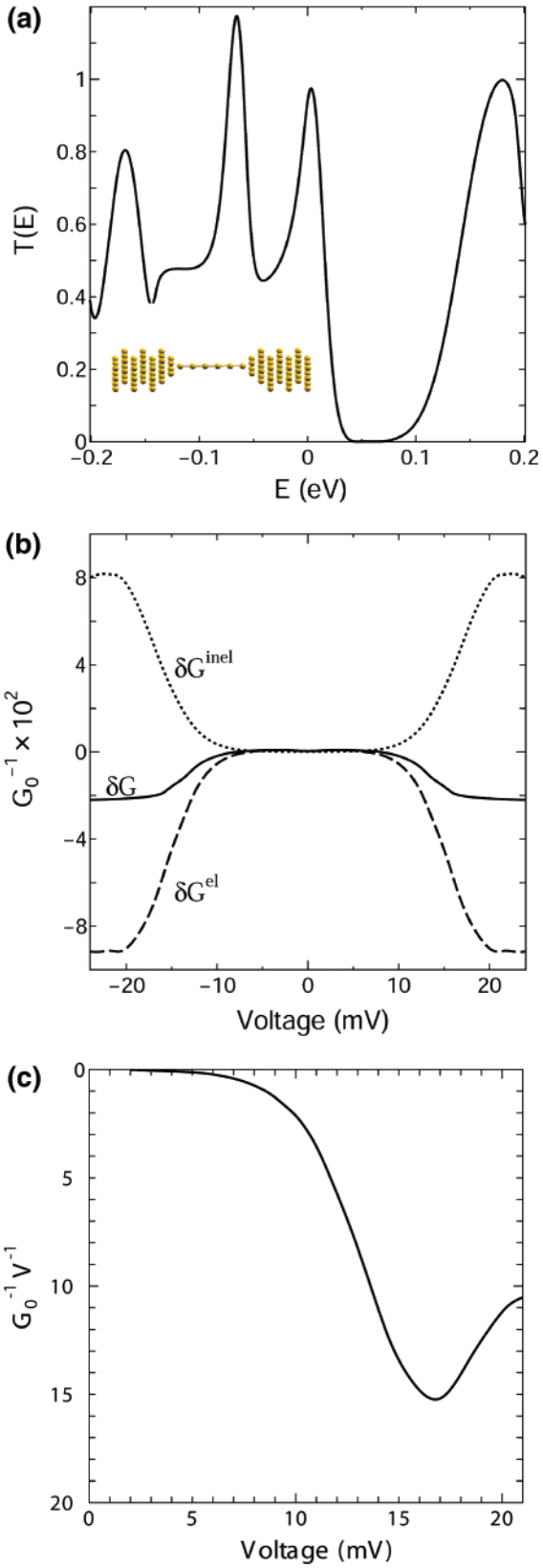

Figure 4. (a) The coefficient $T_0(E)$ and (b) the change of the conductance and (c) the IETS signal in model (III). The notations in the figures are the same as those for Figure 2.

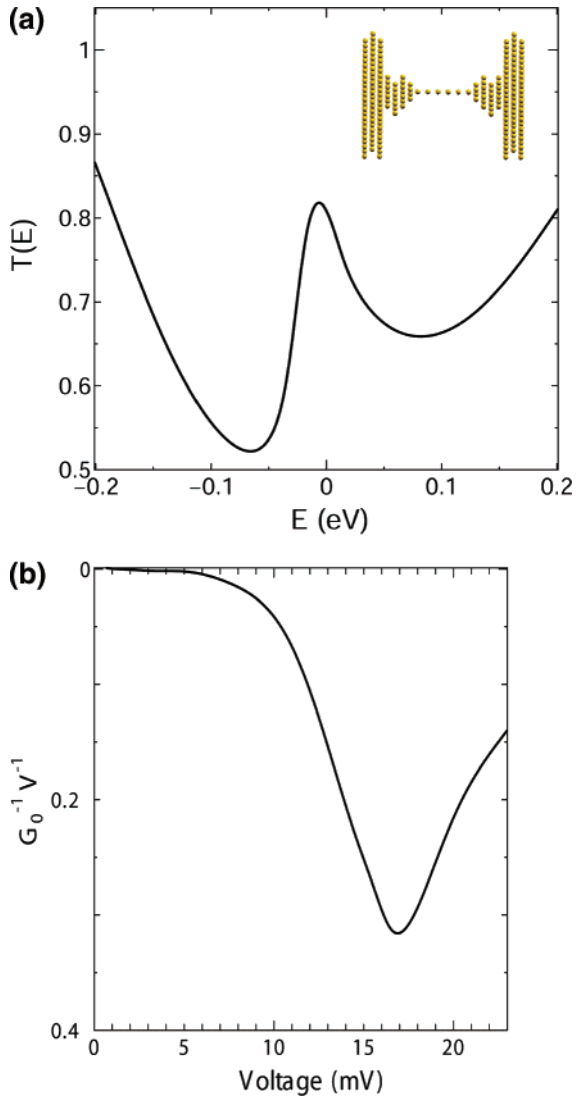

Figure 5. (a) The coefficient $T_0(E)$ and (b) the IETS signal in model (II), where the unit cell has a 4 × 4 structure. The inset in (a) represents a schematic figure to emphasize the relation between the physical model and boundary condition, which is the same with Figures 2−4, but the cross section is 4 × 4.

For models (II) and (III), relating physical systems are different between the 3 × 3 and 4 × 4 sizes because this cell size corresponds to the width of a finite cross section or rod for perpendicular to the transport. First, we show the comparison for model (II). The transmission coefficient fluctuates just as in the case of 3 × 3, although the two results are somewhat different, as shown in Figure 5a. Therefore, the 3 × 3 and 4 × 4 finite cross sections should be distinguished physically and are not a good approximation for a 2-D periodic system, that is, waveguide effects in the connected part between semi-infinite electrodes and finite contacts are still important even if the cross section is of 4 × 4 width as long as the finite cross section part is sufficiently long. On the other hand, the two IETS signals are quite similar, just as shown in Figure 5b. This agreement is reasonable because the electron−phonon couplings are similar (due to its local property), and various T− functions such as T^{ec} take values close to the ones of 4 × 4 in the energy window corresponding to the applied voltage. Just

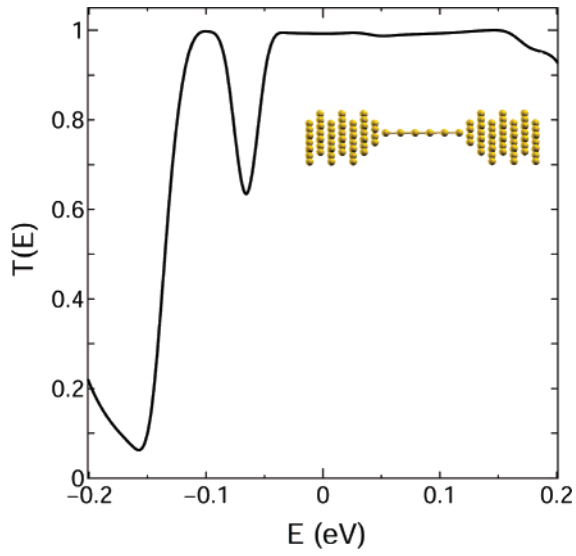

Figure 6. The coefficient $T_0(E)$ for the 4 × 4 unit cell in model (III). The inset represents the related physical system, that is, the 4 × 4 1-D rod.

as the transmission coefficient, their values show smooth and small fluctuation; thus, the difference will not be negligible if a higher voltage than that in the present case is required to get IETS signals. In the present case, the waveguide effect caused by existence of the finite cross section is insensitive to the width of the cross section.

Next, we analyze the 4 × 4 system in model (III). Upon increasing the size of the 1-D rod, one can expect that it approaches the 2-D periodic system, and this justifies the use of a cluster model for the transport problem. Our results actually show that the 4 × 4 rod is much closer to model (I) (i.e., the 2-D periodic case) than the 3 × 3 rod, and the value of $T_0(E)$ is almost the same with the 2-D periodic system. However, a notable drop of the transmission coefficient is found at 0.15 eV below Fermi level, as shown in Figure 6; thus, the 4 × 4 rod is not sufficient to model the 2-D periodicity. It is interesting to consider the cell size dependence with a comparison of models (II) and (III). Although taking a larger cell (3 × 3 ⟹ 4 × 4) improves the fluctuated structure of $T_0(E)$ drastically in model (III), improvement for model (II) is much slower. This leads to the result that the size effect is most obvious result of quantum confinement for the dimensionality of the whole system to determine properties of electron transport. With increasing surface width (cell size), more transverse electronic modes can be included in transport as well as leads (electrodes), and interference caused by transverse wavevectors, which do not satisfy the Bloch condition (in other words, phase mismatching), can be "washed out". On the other hand, the transmission coefficient, as well as the IETS signal, is much more insensitive to the width of the part of the finite cross section, while the length of the cross section is sufficient to provide a difference from the 2-D infinite periodic contact. Fluctuation in model (II) is caused by interference of transverse modes between the cross section and 2-D leads as well as insufficient "washing out" of transverse electronic modes in the cross section. Comparing the above insufficient "washing

out", the type of 1-D/2-D interference is slightly difficult to eliminate by changing the size of the (1-D) unit cell of the cross section, although the resulting fluctuation (e.g., oscillation of the transmission coefficient) is smaller than the fluctuation of quantum confinement of the 1-D system. Therefore, one should classify waveguide effects into the above two mechanisms of interference.

The calculated IETS signal for the 4×4 1-D rod is almost the same as that for the 2-D periodic one, and this agreement is acceptable because of the rapid improvement of fluctuation of T-functions at the Fermi level described above. As a result, the IETS signal is useful data to observe the contribution of waveguide effects to electron−phonon scatterings to prove that whether the system has a long finite cross section or not; particularly, the target is in the low voltage regime because the width of the finite cross section is not so important. Again, we emphasize that existence of a finite cross section is a quite common physical situation such as the MCBJ or STM experiment, and the sensitivity of the IETS signal by waveguide effects could be a useful measurement.

Conclusions. We have presented NEGF-DFT calculations for a gold atomic wire. Our focus is quantum confinement by a finite cross section, and we employed three model systems, (I)−(III), with a change of the size of the unit cell. The waveguide effects for a 1-D rod or finite cross section, which has long length and small width, lead to fluctuations in $T_0(E)$ and changes of δG by electron−phonon scattering, although the differences in coupling coefficients are relatively small between these models.

The key quantity is the wavevector of an electronic transverse mode, that is, the phase factor of the one-electron wave function. The narrow 1-D rod system (e.g., the 3×3 in model (III)) has (nonperiodic, oscillating) electronic transverse modes accessible to the bridge, and interference among them cannot be sufficiently washed out; thus, the sharpest oscillation for $T_0(E)$ and the most strongly enhanced δG are obtained. Furthermore, a strong IETS signal can be found, although electron−phonon couplings are not enhanced compared to the 2-D system. With the increasing width of the rod, interference is rapidly washed out. The IETS signal and the δG values approach the values of the 2-D periodic system also rapidly.

For the finite cross section, effects by the above interference become small, but interference at the connected region between the contact and electrodes will remain. This kind of interference can be expected to be more insensitive to an increase of the unit cell size than the interference in the 1-D rod. Therefore, quantum confinement should be considered when quantities relating to electron−phonon scatterings (e.g, IETS signal) are analyzed. From the viewpoint of theoretical calculations, the present analysis demonstrates the importance of correct estimations for both the C region and lead self-energies with suitable boundary conditions to satisfy "phase matching" to a model realistic system.

Acknowledgment. This research was supported by a Grant-in-Aid for Scientific Research on Priority Area # 18041004 from the Ministry of Education, Culture, Sports, Science, and Technology of Japan. The authors thank the Computer Center of the Institute for Molecular Science for the use of its computers.

References

(1) Aviran, A.; Ratner, M. A. *Molecular Electronics: Science and Technology*; New York Academy of Sciences: New York, 1998.
(2) Blum, A. S.; Kushmerick, J. G.; Pollack, S. K.; Yang, J. C.; Moore, M.; Naciri, J.; Shashidhar, R.; Ratna, B. R. *J. Phys. Chem. B* **2004**, *108*, 18124.
(3) Nitzan, A.; Ratner, M. A. *Science* **2003**, *300*, 1384.
(4) Reed, M. A.; Zhou, C.; Deshpande, M. R.; Muller, C. J.; Burgin, T. P.; Jones, L.; Tour, J. M. *Mol. Electron.: Sci. Technol.* **1998**, *852*, 133.
(5) Reed, M. A.; Zhou, C.; Muller, C. J.; Burgin, T. P.; Tour, J. M. *Science* **1997**, *278*, 252.
(6) Lorente, N.; Persson, M.; Lauhon, L. J.; Ho, W. *Phys. Rev. Lett.* **2001**, *86*, 2593.
(7) Lorente, N.; Rurali, R.; Tang, H. *J. Phys.: Condens. Matter* **2005**, *17*, S1049.
(8) Stipe, B. C.; Rezaei, M. A.; Ho, W. *Science* **1998**, *280*, 1732.
(9) Stipe, B. C.; Rezaei, M. A.; Ho, W. *Rev. Sci. Instrum.* **1999**, *70*, 137.
(10) Troisi, A.; Ratner, M. A. *J. Chem. Phys.* **2006**, *125*, 214709.
(11) Troisi, A.; Ratner, M. A. *Nano Lett.* **2006**, *6*, 1784.
(12) Galperin, M.; Beratan, D. N. *J. Phys. Chem. B* **2005**, *109*, 1473.
(13) Ke, L. Q.; van Schilfgaarde, M.; Kotani, T.; Bennett, P. A. *Nanotechnology* **2007**, 18.
(14) Kobayashi, N.; Brandbyge, M.; Tsukada, M. *Phys. Rev. B* **2000**, *62*, 8430.
(15) Paulsson, M.; Frederiksen, T.; Brandbyge, M. *Nano Lett.* **2006**, *6*, 258.
(16) Stokbro, K.; Taylor, J.; Brandbyge, M.; Mozos, J. L.; Ordejon, P. *Comput. Mater. Sci.* **2003**, *27*, 151.
(17) Xue, Y. Q.; Ratner, M. A. *Phys. Rev. B* **2003**, 68.
(18) Untiedt, C.; Bollinger, G. R.; Vieira, S.; Agrait, N. *Phys. Rev. B* **2000**, *62*, 9962.
(19) Brandbyge, M.; Mozos, J. L.; Ordejon, P.; Taylor, J.; Stokbro, K. *Phys. Rev. B* **2002**, *65*, 165401.
(20) Taylor, J.; Guo, H.; Wang, J. *Phys. Rev. B* **2001**, *63*, 245407.
(21) Ke, S. H.; Baranger, H. U.; Yang, W. T. *J. Chem. Phys.* **2005**, *123*, 114701.
(22) Ke, S. H.; Baranger, H. U.; Yang, W. T. *J. Comput. Theor. Nanosci.* **2006**, *3*, 819.
(23) Nakamura, H.; Yamashita, K. *J. Chem. Phys.* **2006**, *125*, 194106.
(24) Rocha, A. R.; Garcia-Suarez, V. M.; Bailey, S.; Lambert, C.; Ferrer, J.; Sanvito, S. *Phys. Rev. B* **2006**, *73*, 085414.
(25) Xue, Y. Q.; Datta, S.; Ratner, M. A. *J. Chem. Phys.* **2001**, *115*, 4292.
(26) Frederiksen, T.; Brandbyge, M.; Lorente, N.; Jauho, A. P. *Phys. Rev. Lett.* **2004**, *93*, 256601.
(27) Paulsson, M.; Frederiksen, T.; Brandbyge, M. *Phys. Rev. B* **2005**, *72*, 201101.
(28) Paulsson, M.; Frederiksen, T.; Brandbyge, M. *Phys. Rev. B* **2007**, *75*, 129901.
(29) Viljas, J. K.; Cuevas, J. C.; Pauly, F.; Hafner, M. *Phys. Rev. B* **2005**, *72*, 245415.
(30) Galperin, M.; Ratner, M. A.; Nitzan, A. *J. Phys.: Condens. Matter* **2007**, *19*, 103201.
(31) Ryndyk, D. A.; Hartung, M.; Cuniberti, G. *Phys. Rev. B* **2006**, *73*.
(32) Nakamura, H.; Yamashita, K. To be submitted.
(33) Agrait, N.; Untiedt, C.; Rubio-Bollinger, G.; Vieira, S. *Phys. Rev. Lett.* **2002**, *88*, 216903.
(34) Agrait, N.; Untiedt, C.; Rubio-Bollinger, G.; Vieira, S. *Chem. Phys.* **2002**, *281*, 231.
(35) Soler, J. M.; Artacho, E.; Gale, J. D.; Garcia, A.; Junquera, J.; Ordejon, P.; Sanchez-Portal, D. *J. Phys.: Condens. Matter* **2002**, *14*, 2745.
(36) Thygesen, K. S.; Jacobsen, K. W. *Phys. Rev. B* **2005**, *72*, 033401.
(37) de la Vega, L.; Martin-Rodero, A.; Agrait, N.; Yeyati, A. L. *Phys. Rev. B* **2006**, *73*, 075428.

NL071281C